Coronary Plaque Microstructure and Composition Modify Optical Polarization:

A New Endogenous Contrast Mechanism for Optical Frequency Domain Imaging

Martin Villiger, PHD[a], **Kenichiro Otsuka, MD, PHD**[a], **Antonios Karanasos, MD, PHD**[b], **Pallavi Doradla, PHD**[a], **Jian Ren, PHD**[a], **Norman Lippok, PHD**[a], **Milen Shishkov, PHD**[a], **Joost Daemen, MD**[b], **Roberto Diletti, MD**[b], **Robert-Jan van Geuns, MD, PHD**[b], **Felix Zijlstra, MD, PHD**[b], **Gijs van Soest, PHD**[b], **Peter Libby, MD**[c], **Evelyn Regar, MD, PHD**[b], **Seemantini K. Nadkarni, PHD**[a], and **Brett E. Bouma, PHD**[a,d]

[a]Wellman Center for Photomedicine, Massachusetts General Hospital, Harvard Medical School, Boston, Massachusetts [b]Department of Interventional Cardiology, Thoraxcenter, Erasmus Medical Center, Rotterdam, the Netherlands [c]Division of Cardiovascular Medicine, Department of Medicine, Brigham and Women's Hospital, Harvard Medical School, Boston, Massachusetts [d]Institute for Medical Engineering and Science, Massachusetts Institute of Technology, Cambridge, Massachusetts

Abstract

OBJECTIVES—This study aimed to evaluate whether polarimetry, performed using a modified optical frequency domain imaging (OFDI) system, can improve the assessment of histological features relevant to characterizing human coronary atherosclerosis.

BACKGROUND—The microscopic structure and organization of the arterial wall influence the polarization of the infrared light used by OFDI. Modification of the OFDI apparatus, along with recently developed image reconstruction methods, permits polarimetric measurements simultaneously with conventional OFDI cross-sectional imaging through standard intravascular imaging catheters.

METHODS—The main coronary arteries of 5 cadaveric human hearts were imaged with an OFDI system capable of providing polarimetric assessment. Cross-sectional views of tissue birefringence, measured in refractive index units, and depolarization, expressed as the ratio of depolarized signal to total intensity, were reconstructed, together with conventional OFDI images. Following imaging, the vessels underwent histological evaluation to enable interpretation of the observed polarization features of individual tissue components.

RESULTS—Birefringence in fibrous tissue was significantly higher than in intimal tissue with minimal abnormality (0.44×10^{-3} vs. 0.33×10^{-3}; p < 0.0001). Birefringence was highest in the

ADDRESS FOR CORRESPONDENCE: Dr. Martin Villiger, Wellman Center for Photomedicine, Massachusetts General Hospital, 50 Blossom Street, Boston, Massachusetts 02114. mvilliger@mgh.harvard.edu.

tunica media (p < 0.0001), consistent with its high smooth muscle cell content, cells known to associate with birefringence. In fibrous areas, birefringence showed fine spatial features and close correspondence with the histological appearance of collagen. In contrast, necrotic cores and regions rich in lipid elicited significant depolarization (p < 0.0001). Depolarization was also evident in locations of cholesterol crystals and macrophages.

CONCLUSIONS—Intravascular measurements of birefringence and depolarization can be obtained using conventional OFDI catheters in conjunction with a modified console and signal processing algorithms. Polarimetric measurements enhance conventional OFDI by providing additional information related to the tissue composition and offer quantitative metrics enabling characterization of plaque features.

Keywords

cholesterol crystals; collagen; optical coherence tomography; optical frequency domain imaging; polarized light

Fatal coronary thrombosis frequently results from the rupture of plaques that have a large lipid core, separated from the lumen by a thin fibrous cap (1,2). Plaque erosion accounts for most of the remainder of coronary thrombotic events and involves the formation of a thrombus on the eroded intima of a lesion that lacks a large lipid core (1,2). Expanding on autopsy studies, the advent of invasive imaging with intravascular catheters has afforded considerable insight into the mechanisms of coronary events (3). Prospective clinical imaging studies suggest that few thin-capped fibroatheromas actually precipitate acute thrombosis (4), and many aspects of coronary thrombotic occlusion remain vigorously debated (5). Optical coherence tomography (OCT) (6) and optical frequency domain imaging (OFDI) (7) currently offer the highest spatial resolution for intravascular imaging, enable the assessment of fibrous cap thickness (8), and elucidate aspects of plaque erosion (9). Despite the merits of contemporary intravascular imaging, there remains a need for improved imaging methods to characterize plaque morphology and composition more accurately. The detection of fluorescence emitted from characteristic plaque components or injectable fluorescent labels has been investigated to complement OCT and enhance plaque characterization (10,11). Near-infrared spectroscopy (12) and photoacoustic imaging (13,14) have also shown promise and complement intravascular ultrasound and OCT, but these approaches require custom multimodal imaging catheters that complicate clinical translation (15).

The present work aimed to investigate the distinct signatures that different atherosclerotic plaque components impart on the polarization of infrared light as used by intravascular OFDI. Tissue with fibrillar architecture, such as interstitial collagen or layered arrays of arterial smooth muscle cells (SMCs), exhibits birefringence, an optical property that results in a differential delay, or retardation, between light polarized parallel to the tissue fibrillar components and light having a perpendicular polarization. Nadkarni et al. (16) previously established that birefringence is well correlated with collagen and SMC content. This was demonstrated in aortic plaques, which appear spatially homogenous on a microscopic scale and when a conventional polarization-sensitive (PS) OCT microscope is used. Meaningful intravascular polarization measurements through a catheter have not been possible, however,

because the bending and rotation of the optical fiber in the catheter induce severe polarization distortions (17). Given the recently developed reconstruction strategies that mitigate the resulting artifacts (18), we demonstrate here the ability to measure depth-resolved birefringence and an additional quantitative metric, depolarization, through standard intravascular imaging catheters. Evaluating birefringence locally at each depth is essential for imaging the layered architecture of coronary arteries and offers an important advance over our earlier work (16). Depolarization corresponds to a randomization of the detected polarization states and complements birefringence for the polarimetric characterization of tissue (18). We hypothesized that assessment of depolarization for intravascular imaging could offer additional insights and enhance the characterization of atherosclerotic plaques.

Here we present an evaluation of human coronary arteries with intravascular polarimetry. We imaged the coronary arteries of human cadaver hearts with PS-OFDI and prepared co-registered histological sections. We then established an atlas of polarization signatures of various plaque components and explored the ability of this contrast mechanism to refine plaque characterization.

METHODS

POLARIZATION-SENSITIVE OPTICAL FREQUENCY DOMAIN IMAGING SYSTEM

Imaging of cadaveric hearts used a custom-built state-of-the-art OFDI apparatus and 2.6-F intravascular catheters. Figures 1A to 1E illustrate the principle of PS imaging (details in the Online Methods section). Cadaveric coronary arteries were imaged with 2,048 A-lines (radial scans) per rotation, thus yielding 1,024 A-lines for each of the 2 alternating input polarization states. The pull back speed of 5 mm/s was adjusted to achieve longitudinal sampling with a 100-μm pitch.

RECONSTRUCTION OF TISSUE BIREFRINGENCE AND DEPOLARIZATION

Birefringence is the unitless ratio of retardation per propagation distance. It corresponds to the difference,   n, of the refractive indices experienced by light polarized parallel and orthogonal to the fibrillary components. Birefringence maps were reconstructed with spectral binning (18) (details in the Online Methods) and are displayed in the range of 0 to 1.8×10^{-3}. Areas of high depolarization, which precludes the reconstruction of meaningful birefringence, are omitted from the maps (details in the Online Methods).

Depolarization corresponds to a randomization of the detected polarization states within a small neighborhood around each pixel. It is expressed as the ratio of the depolarized signal to the total intensity (18) (details in the Online Methods). In practice, depolarization values range from 0 (no depolarization) to ~0.5, corresponding to regions where the OFDI signal falls to the noise floor. Depolarization is displayed in the range of 0.0 to 0.5 throughout this study.

CADAVERIC HEARTS AND IMAGING PROCEDURE

The National Disease Research Interchange provided 5 cadaveric human hearts (from 4 men and 1 woman), delivered fresh in phosphate buffered saline. The times between death and imaging ranged from 24 to 72 h. The average age at death was 63 ± 11 years. The cause of death was cardiac in 3 cases. Imaging of the cadaveric hearts used a 6-F guide catheter and a 0.014-inch guidewire in a conventional manner. We imaged a total of 10 vessels, including the left anterior descending coronary artery in all, the right coronary artery in 3, and the left circumflex coronary artery (LCx) in 2 hearts, with a cumulative pull back length of ~700 mm. Some coronary arteries could not be catheterized because of severe calcifications and/or tortuosity and were not imaged. After deploying the imaging catheter, the guidewire was withdrawn to avoid shadowing artifacts in the OFDI images. During the pull back, phosphate buffered saline was perfused through the guide catheter. Following imaging, the coronary arteries were resected from the heart and pressure fixed in 10% buffered formalin.

HISTOPATHOLOGICAL EXAMINATION AND DIGITAL IMAGE ACQUISITION

After reviewing the acquired OFDI data, we defined 49 vessel segments 5 to 10 mm in length, having atherosclerosis for subsequent histological processing, excluding vessel areas with only minimal abnormality or stents. The fixed segments were decalcified, embedded in paraffin, and cut into 5-μm thick sections at a level spacing of 500 μm, yielding a total 756 levels. Serial sections were collected and stained with hematoxylin and eosin. Corresponding OFDI cross sections were identified in the conventional OFDI images using visual landmarks such as side branches, plaque morphology, and calcifications. Given the short level spacing of 500 μm, the circumferential orientation and position along the pull back of sections without identifying features could be derived relative to matched neighboring sections. Excluding adjacent cross sections that featured similar lesion morphology, we retained a selection of 100 sections, categorized into adaptive intimal thickening (n = 13), pathological intimal thickening (n = 45), fibrous plaques (n = 12), fibrocalcified plaques (n = 13), and fibroatheromas (n = 17). Selected slides were further stained with Masson trichrome and picrosirius red (PSR) for assessment of collagen architecture and content, α-smooth muscle actin (SMA) for SMCs, or CD68, a macrophage marker. All but the PSR-stained sections were digitized with a whole slide scanning system (Nanozoomer 2.0-RS, Hamamatsu, Middlesex, New Jersey). PSR-stained sections were imaged with a polarized light microscope (BX43, Nikon, Center Valley, Pennsylvania) that used circularly polarized light to provide maps of collagen content (19).

QUANTITATIVE TISSUE CHARACTERIZATION

To compare the polarimetric signals among different tissue types, we manually segmented the lumen contour in the 100 matching cross sections. We also segmented the internal elastic lamina, on the basis of the OFDI reflectivity signal whenever visible, and extrapolated from the matching histology sections otherwise. Next, the tissue between the lumen and the internal elastic lamina was divided into angular segments and categorized into 1 of the following 4 tissue types: normal intima, fibrous tissue, early lesions, and advanced lesions. Intima was defined as intimal tissue with minimal disease with a thickness inferior or equal to that of the tunica media. Fibrous tissue corresponds to areas of increased intimal

thickening or cross sections through fibrotic areas of advanced plaques. Early lesions comprise fatty streaks and pathological intimal thickening, exhibiting changes in the extracellular matrix, foamy macrophages, and only dispersed extracellular lipid. Advanced lesions contain large pools of extracellular lipid or necrotic cores and correspond to advanced pathological intimal thickening and fibroatheromas. In addition, calcifications and the tunica media were also segmented whenever they were clearly visible in the OFDI reflection signal. The inset in Figure 2A shows an example of the resulting tissue type segmentation. The median birefringence in areas with a depolarization   0.2 and the median depolarization throughout the entire segments were then computed for each tissue segment.

STATISTICAL METHODS

Statistical analysis was performed using MATLAB (The MathWorks, Inc., Natick, Massachusetts). The polarimetry signals of the different tissue types were evaluated for statistically significant variation with 1-way analysis of variance for birefringence, and the Kruskal-Wallis test for depolarization, which was non-normally distributed. Pairwise comparison was performed with the Tukey honestly significant difference procedure. Differences were considered significant at values of $p < 0.05$. No adjustments were made for correlated observations within individuals.

RESULTS

Figure 1 summarizes the modifications necessary to enable an OFDI system to perform intravascular PS measurements and to recover maps of tissue birefringence and depolarization in addition to the conventional reflection signal. Because of the compatibility with commercial clinical intravascular catheters, we previously performed initial clinical imaging (20). Figure 1 demonstrates features of birefringence and depolarization in the LCx of a 52-year-old male patient who presented with stable angina. To interpret these rich signatures, we conducted PS-OFDI of cadaver hearts and compared the results with histological examination of matching tissue sections. Figures 2A to 2I display a representative cross section of a fibroatheroma, exhibiting the characteristic polarization signatures observed throughout all imaged coronary arteries.

MINIMAL DISEASE

From 11 to 2 o'clock, the cross section in Figure 2 exhibits features of minimal abnormality. The intimal layer in this segment has low birefringence and contrasts with the increased birefringence detected in the tunica media. The birefringence in the adventitia remains high in this section, and a fine line of low birefringence separates the 2 layers. Other cross sections show a return to a lower birefringence in the adventitia (e.g., Figure 1D, from 8 to 11 o'clock). Depolarization remains very low throughout the entire vessel wall and increases only in the periadventitial fat, where the irregular scattering of light by adipose cells scrambles the polarization states.

The corresponding histological section reveals densely packed SMCs in the tunica media (Figures 2F and 2I). The intimal layer of human arteries also contains cells that stain positive

for SMA. Unlike the SMCs in the media, however, these cells express SMA more focally and appear less regularly arrayed.

FIBROUS TISSUE

The conventional OFDI reflection signal exhibits only a modest variation across fibrous intimal tissue (2 to 4 and 9 to 11 o'clock in Figure 2A) and the fibrous cap. In comparison, the birefringence signal reveals layers and zones of varying and increased birefringence (Figure 2B), thus suggesting distinct tissue architecture. Depolarization remains low throughout fibrous regions and increases only at the outer boundary of the adventitia or at the edge of the fibrous cap (Figure 2C). Fibrous lesions primarily consist of collagen, and we compared the PS-OFDI signal with co-registered histological sections stained with trichrome and PSR. Consistent with the birefringence maps, the PSR staining reveals layers and regions of varying collagen morphology (Figures 2E and 2H). Areas of strong PSR signal correspond closely to regions of increased birefringence by PS-OFDI. Both the PS-OFDI and PSR signal suggest reduced collagen content at the right shoulder of the fibrous cap. Such features have importance because they may correspond to sites of mechanical weakness.

LIPID-RICH PLAQUES AND NECROTIC CORES

In OFDI, plaques with lipid pools or necrotic cores exhibit rapid reflection signal drop-off with poorly delineated borders (6). PS-OFDI consistently exhibited very pronounced depolarization in regions corresponding to necrotic core material, extracellular accumulation of lipid, or lipid-laden foam cells by histopathology. In Figure 2C, the depolarization signal starts to increase from its low baseline value precisely at the border of the fibrous cap and the underlying necrotic core, thereby offering a clear, objective delineation of the cap. Figures 3A to 3E show additional examples suggesting that progressive accumulation of lipid results in increased depolarization. Early accumulation of lipid and individual scattered foam cells causes only modest depolarization, in contrast to the abrupt depolarization of a large pool of foam cells.

CALCIFICATIONS

The OFDI reflection signal readily identifies zones of calcifications because they appear translucent and have sharp borders (6). In PS-OFDI, calcium mineral accumulations tend to depolarize, more so in lipid-rich plaques than in fibrocalcified plaques without lipid (Figures 4A to 4E). Calcifications appear to disturb the birefringence of the underlying tissue substrate, as also manifested by a reduction or absence of the PSR signal within the calcified regions (Figure 4E).

CHOLESTEROL CRYSTALS AND MACROPHAGES

In addition to the tissue components discussed earlier, we found evidence for polarization signatures caused by cholesterol crystals and macrophages. Figures 5A to 5E, rows 1 and 2, show collections of cholesterol crystals that cause pronounced depolarization. Some crystals in Figures 5A to 5E, row 2, appear to align parallel to the lumen and produce a linear reflection signal, surrounded by spots of high birefringence. Macrophages may yield a

spotty appearance in OFDI reflection images (21), and criteria to delineate automatically macrophage-rich regions exist (22). Figures 5A to 5E, rows 3 and 4, indicate that isolated accumulations of macrophages can generate a subtle depolarization.

QUANTITATIVE CHARACTERIZATION OF TISSUE POLARIZATION PROPERTIES

Both birefringence and depolarization differ significantly ($p < 0.0001$) among the analyzed tissue groups (Figures 6A and 6B). Consistent with the visual appearance, quantitative analysis revealed that the tunica media features significantly higher birefringence than all other tissue types ($p < 0.0001$). Intimas with minimal abnormality have significantly lower birefringence than all other tissues ($p < 0.05$), except for calcifications ($p = 0.068$). Birefringence was analyzed only in areas where depolarization was 0.2, thus excluding areas where birefringence cannot be evaluated reliably. In advanced lesions with a defined lipid pool or a necrotic core, these nondepolarizing areas correspond approximately to the fibrous caps and exhibit lower birefringence than in early lesions with dispersed lipid, albeit without statistical significance (0.44×10^{-3} vs. 0.51×10^{-3}; $p = 0.17$). Early lesions show a slightly but significantly higher birefringence than fibrous tissue (0.51×10^{-3} vs. 0.44×10^{-3}; $p < 0.05$). Intimal and fibrous tissues, as well as the media, have low depolarization, contrasting with the significantly higher depolarization of lipid-containing plaques and calcifications ($p < 0.0001$). Although without statistical significance, advanced lipid pools show higher depolarization than less mature lipidrich plaques (0.41 vs. 0.19; $p = 0.226$).

DISCUSSION

This study demonstrates intracoronary polarimetry with PS-OFDI. Polarimetric imaging of human coronary arteries ex vivo and comparison with corresponding histological features revealed rich birefringence features in fibrous tissue with a spatial distribution considerably finer than in aortic plaques, thus suggesting a more complex spatial distribution of collagen and smooth muscle in the coronary arteries compared with the aorta (16). Our data evidenced a high birefringence of the tunica media, contrasting with the intima and adventitia, as well as pronounced depolarization of lipid and necrotic core material. The improved conspicuity of the media may provide a more robust assessment of the dimension of the external elastic membrane compared with conventional OFDI. Depolarization could serve as a quantitative metric to determine fibrous cap thickness reliably and automatically. Although our results do not conclusively demonstrate an improved ability to characterize thin-capped fibroatheromas, our polarization metrics may offer additional insights into aspects of plaque stability in the future.

From a practical perspective, PS-OFDI is performed in a manner identical to that of conventional OFDI, uses the same catheters, and imposes no additional constraint on the imaging procedure. A simple modification of the imaging engine and advanced post-processing enable the investigation of this intrinsic polarization contrast.

Both SMC and collagen are known to exhibit birefringence (16,23). The high abundance of SMCs in the tunica media suggests that these cells embedded in their extracellular matrix envelopes cause the high birefringence observed in this layer. In fibrous regions of the arterial intima, collagen appears to contribute most to the observed birefringence because

these regions contain only few and scattered SMCs. Our results show good correspondence between birefringent features and collagen in these areas, as assessed with PSR histochemical localization. In addition, birefringence has previously been shown to correlate with collagen content in excised aortic tissue (16). The fine spatial organization of birefringence features in coronary atherosclerosis prevented a detailed correlation between histological features and intravascular PS-OFDI in the current study.

Birefringence is a directional property, defined by the orientation of collagen and muscle fibers. PS-OFDI measures birefringence only for the component of the fibers running approximately orthogonal to the probing beam (i.e., circumferential or longitudinal along the vessel). Fibers that orient radially yield only minimal birefringence. Conveniently, such an orientation is uncommon for fibers in the vessel wall.

The physical origin of the pronounced depolarization in lipid-rich areas is unclear. We speculate that it relates to strong optical scattering and random arrangement of intracellular and extracellular lipid droplets and potentially crystalized cholesterol. The clinical significance of lipid-rich plaques has recently been demonstrated (24); however, identification of lipid pools, especially when they localize deeper in the plaque, can be ambiguous on the basis of the reflection signal alone (25). Depolarization may offer a novel metric to detect lipid-rich areas reliably and automatically.

Cholesterol crystals also caused depolarization of infrared light, occasionally with associated regions of birefringence. These observations are consistent with the known birefringence and dimensions of cholesterol crystals (26): plaque regions where small cholesterol crystals are present without organized alignment should give rise to depolarization; regions with some degree of alignment should exhibit birefringence by PS-OFDI. In conventional OFDI, cholesterol crystals can produce linear, highly reflective signals. Confusion with microcalcifications is possible, however, and the additional polarization signatures may improve their identification and assessment. Regions of macrophage accumulation similarly were associated with subtle depolarization, which could aid the automatic detection of macrophage-rich areas (21,22).

Quantitative analysis of the polarization metrics revealed significant differences among several histologically identified tissue types. The specific composition of tissue influences the polarization of near-infrared light and causes characteristic polarization properties for some tissues. PS-OFDI provides additional tissue differentiation, particularly in plaque areas that appear relatively homogeneous or isointense in the reflection signal. Our analysis included all intimal and identifiable medial tissue segments across the available cross sections, and this inclusion underlines the robustness of the observed signatures. The significant difference between tissue types and the formulation of the polarization properties as absolute metrics may enable automated plaque assessment, including medial border segmentation or tissue classification, which are topics of ongoing research. Differences among heterogeneous plaque components (early or advanced lesions and calcium) were less pronounced because of the intrinsic variability in these categories.

STUDY LIMITATIONS

Limitations of this work include the study of paraffin-embedded sections, which precluded staining for lipid with Oil Red O. The common ethanol fixation protocols also dissolve cholesterol crystals (27), thus leading to the typical clefts for large crystals, but they exclude the assessment of smaller or intracellular crystals. Preliminary clinical data suggest that PS-OFDI may help in assessing thrombus material (20), but such tissue was absent from our autopsy dataset. The frame rate and pull back speed for PS-OFDI used in this study were lower than those of contemporary clinical OFDI to facilitate matching with histological appearance. We do not anticipate, however, that an increased frame rate and pull back speed would substantially have influenced the reconstruction of tissue polarization properties.

CONCLUSIONS

This study demonstrates the ability and prospects of intravascular polarimetry with PS-OFDI for the characterization of coronary arterial atherosclerotic lesions. In addition to the cross-sectional image of arterial microstructure, PS-OFDI measures polarization properties that facilitate assessment of vessel morphology and offer further insight into plaque composition. These metrics may improve our mechanistic understanding of plaque progression and the pathogenesis of acute coronary events and could lead to a lesion-specific, more personalized risk stratification and assessment of plaque stability.

Supplementary Material

Refer to Web version on PubMed Central for supplementary material.

Acknowledgments

ABBREVIATIONS AND ACRONYMS

LCx	left circumflex coronary artery
OCT	optical coherence tomography
OFDI	optical frequency domain imaging
PS	polarization sensitive
PSR	picrosirius red
SMA	α-smooth muscle actin
SMC	smooth muscle cell

References

1. Virmani R, Burke AP, Farb A, Kolodgie FD. Pathology of the vulnerable plaque. J Am Coll Cardiol. 2006; 47(Suppl):C13–8. [PubMed: 16631505]

2. Libby P. Mechanisms of acute coronary syndromes and their implications for therapy. N Engl J Med. 2013; 368:2004–13. [PubMed: 23697515]

3. Batty JA, Subba S, Luke P, Gigi LW, Sinclair H, Kunadian V. Intracoronary imaging in the detection of vulnerable plaques. Curr Cardiol Rep. 2016; 18:28. [PubMed: 26879196]

4. Stone GW, Maehara A, Lansky AJ, et al. A prospective natural-history study of coronary atherosclerosis. N Engl J Med. 2011; 364:226–35. [PubMed: 21247313]

5. Libby P, Pasterkamp G. Requiem for the 'vulnerable plaque.'. Eur Heart J. 2015; 36:2984–7. [PubMed: 26206212]

6. Jang IK, Bouma BE, Kang DH, et al. Visualization of coronary atherosclerotic plaques in patients using optical coherence tomography: comparison with intravascular ultrasound. J Am Coll Cardiol. 2002; 39:604–9. [PubMed: 11849858]

7. Yun SH, Tearney GJ, Vakoc BJ, et al. Comprehensive volumetric optical microscopy in vivo. Nat Med. 2006; 12:1429–33. [PubMed: 17115049]

8. Kume T, Akasaka T, Kawamoto T, et al. Assessment of coronary arterial thrombus by optical coherence tomography. Am J Cardiol. 2006; 97:1713–7. [PubMed: 16765119]

9. Jia H, Abtahian F, Aguirre AD, et al. In vivo diagnosis of plaque erosion and calcified nodule in patients with acute coronary syndrome by intravascular optical coherence tomography. J Am Coll Cardiol. 2013; 62:1748–58. [PubMed: 23810884]

10. Kim S, Lee MW, Kim TS, et al. Intracoronary dual-modal optical coherence tomography-near-infrared fluorescence structural-molecular imaging with a clinical dose of indocyanine green for the assessment of high-risk plaques and stentassociated inflammation in a beating coronary artery. Eur Heart J. 2016; 37:2833–44. [PubMed: 26787442]

11. Ughi GJ, Wang H, Gerbaud E, et al. Clinical characterization of coronary atherosclerosis with dual-modality OCT and near-infrared auto-fluorescence imaging. J Am Coll Cardiol Img. 2016; 9:1304–14.

12. Madder RD, Goldstein JA, Madden SP, et al. Detection by near-infrared spectroscopy of large lipid core plaques at culprit sites in patients with acute ST-segment elevation myocardial infarction. J Am Coll Cardiol Intv. 2013; 6:838–46.

13. Zhang J, Yang S, Ji X, Zhou Q, Xing D. Characterization of lipid-rich aortic plaques by intravascular photoacoustic tomography. J Am Coll Cardiol. 2014; 64:385–90. [PubMed: 25060374]

14. Wu M, Springeling G, Lovrak M, et al. Real-time volumetric lipid imaging in vivo by intravascular photoacoustics at 20 frames per second. Biomed Opt Express. 2017; 8:943–53. [PubMed: 28270995]

15. Bourantas CV, Garcia-Garcia HM, Naka KK, et al. Hybrid intravascular Imaging. J Am Coll Cardiol. 2013; 61:1369–78. [PubMed: 23500282]

16. Nadkarni SK, Pierce MC, Park BH, et al. Measurement of collagen and smooth muscle cell content in atherosclerotic plaques using polarization-sensitive optical coherence tomography. J Am Coll Cardiol. 2007; 49:1474–81. [PubMed: 17397678]

17. Villiger M, Zhang EZ, Nadkarni S, Oh WY, Bouma BE, Vakoc BJ. Artifacts in polarization-sensitive optical coherence tomography caused by polarization mode dispersion. Opt Lett. 2013; 38:923–5. [PubMed: 23503261]

18. Villiger M, Zhang EZ, Nadkarni SK, Oh WY, Vakoc BJ, Bouma BE. Spectral binning for mitigation of polarization mode dispersion artifacts in catheter-based optical frequency domain imaging. Opt Express. 2013; 21:16353–69. [PubMed: 23938487]

19. Whittaker P, Kloner RA, Boughner DR, Pickering JG. Quantitative assessment of myocardial collagen with picrosirius red staining and circularly polarized light. Basic Res Cardiol. 1994; 89:397–410. [PubMed: 7535519]

20. van der Sijde JN, Karanasos A, Villiger M, Bouma BE, Regar E. First-in-man assessment of plaque rupture by polarization-sensitive optical frequency domain imaging in vivo. Eur Heart J. 2016; 37:1932. [PubMed: 27174288]

21. Tearney GJ, Yabushita H, Houser SL, et al. Quantification of macrophage content in atherosclerotic plaques by optical coherence tomography. Circulation. 2003; 107:113–9. [PubMed: 12515752]

22. Phipps JE, Vela D, Hoyt T, et al. Macrophages and intravascular OCT bright spots: a quantitative study. J Am Coll Cardiol Img. 2015; 8:63–72.

23. Wolman M. Polarized light microscopy as a tool of diagnostic pathology. J Histochem Cytochem. 1975; 23:21–50. [PubMed: 1090645]

24. Xing L, Higuma T, Wang Z, et al. Clinical significance of lipid-rich plaque detected by optical coherence tomography: a 4-year follow-up study. J Am Coll Cardiol. 2017; 69:2502–13. [PubMed: 28521888]

25. Kim SJ, Lee H, Kato K, et al. Reproducibility of in vivo measurements for fibrous cap thickness and lipid arc by OCT. J Am Coll Cardiol Img. 2012; 5:1072–4.

26. Zakharova MM, Nasonova VA, Konstantinova AF, Chudakov VS, Gainutdinov RV. An investigation of the optical properties of cholesterol crystals in human synovial fluid. Crystallography Reports. 2009; 54:509–12.

27. Abela GS, Aziz K, Vedre A, Pathak DR, Talbott JD, Dejong J. Effect of cholesterol crystals on plaques and intima in arteries of patients with acute coronary and cerebrovascular syndromes. Am J Cardiol. 2009; 103:959–68. [PubMed: 19327423]

PERSPECTIVES

COMPETENCY IN MEDICAL KNOWLEDGE

The microscopic structure and organization of the arterial wall influence the polarization of infrared light. Collagen and SMCs exhibit birefringence, whereas zones containing lipid, necrotic core material, or macrophages randomize the polarization states of scattered light.

TRANSLATIONAL OUTLOOK

Clinical studies are needed to investigate tissue polarization signatures in the coronary arteries of patients and test whether intravascular polarimetry may be of diagnostic use to identify aspects of plaque stability and enable more personalized risk stratification.
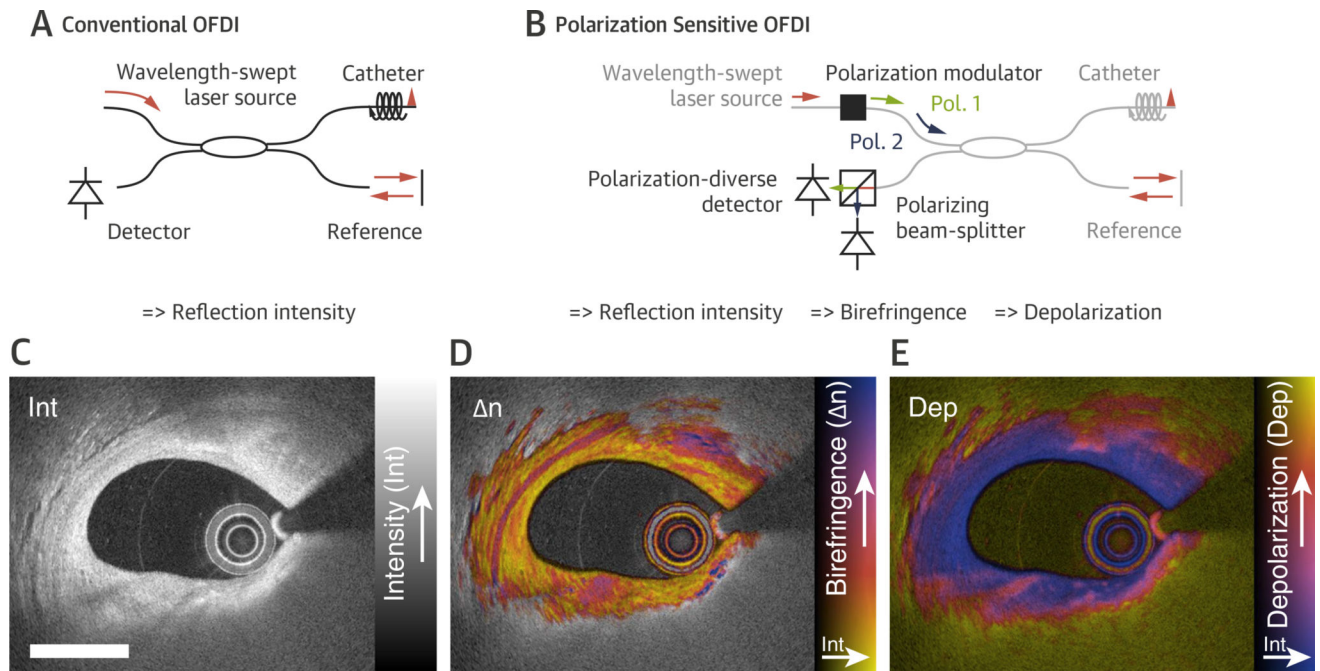
FIGURE 1. Working Principle of PS-OFDI

Polarization-sensitive optical frequency domain imaging (PS-OFDI) is compatible with current intravascular optical frequency domain imaging catheters and enables measurement of tissue polarization properties simultaneously with the conventional reflection intensity. **(A)** In addition to the components of conventional optical frequency domain imaging, polarization-sensitive optical frequency domain imaging uses **(B)** a polarization modulator and detects the light reflected by the tissue along 2 orthogonal polarization states. The modulator alternates the polarization state of the light incident on the tissue between even and odd A-lines. Analyzing the spatial variation of the detected states allows reconstruction of birefringence (Δn) and depolarization (Dep). **(C to E)** Polarization-sensitive optical frequency domain imaging signals measured in vivo in the left circumflex coronary artery of a 52-year-old man. **(C)** Intensity (Int) of the reflection signal showing subsurface plaque morphology in a conventional logarithmic gray scale. **(D)** Birefringence in color hue, overlaid on the reflection signal, revealing regions and layers of distinct birefringence. Birefringence is displayed only in areas of low depolarization. **(E)** Depolarization in color hue, overlaid on the reflection signal, indicating zones of pronounced depolarization. Scale bar: 1 mm.
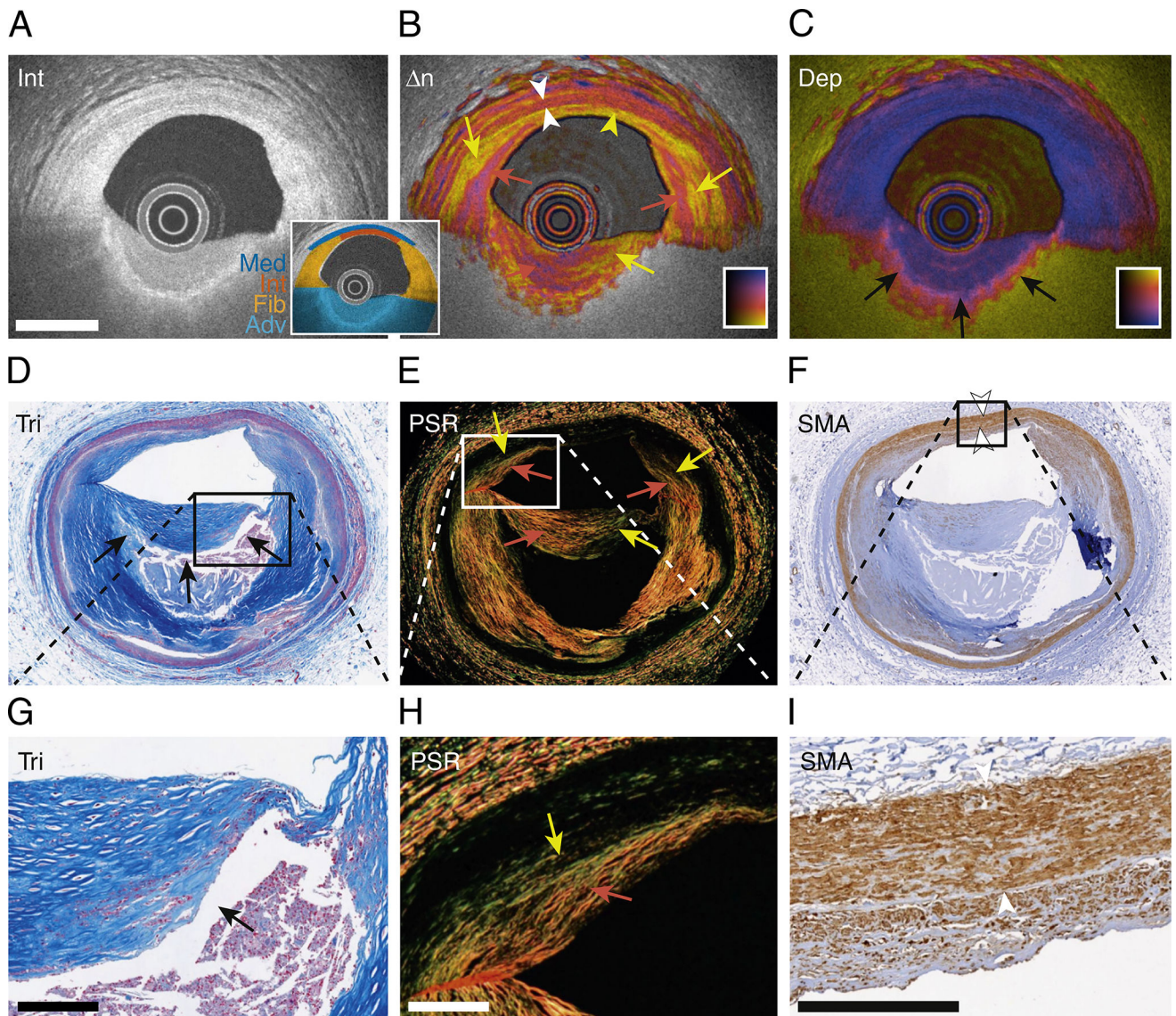
FIGURE 2. PS-OFDI of Fibroatheroma

Individual components of human atherosclerotic plaques and vessel wall ex vivo exhibit distinct polarization features in polarization-sensitive optical frequency domain imaging (PS-OFDI). **(A)** Reflection intensity (Int), **(B)** birefringence (n), **(C)** depolarization (Dep) of a fibroatheroma, and **(D to F)** matching histological sections, stained with trichrome (Tri), picrosirius red (PSR), and α-smooth muscle actin (SMA), respectively. **(G to I)** Magnified views of the regions of interest indicated in **(D to F),** respectively. Intimal tissue in segments of minimal pathology display low birefringence **(yellow arrowhead)**. The media features increased birefringence **(white arrowheads)**, caused most likely by the dense packing of smooth muscle cells. Birefringence in intimal fibrous regions corresponds closely to collagen content, assessed with picrosirius red histology. **Red and yellow arrows** indicate zones of higher or lower birefringence and picrosirius red signals, respectively. The necrotic core causes an abrupt depolarization **(black arrows)**. For quantitative characterization of tissue polarization properties, segments of different tissue types were defined in each cross
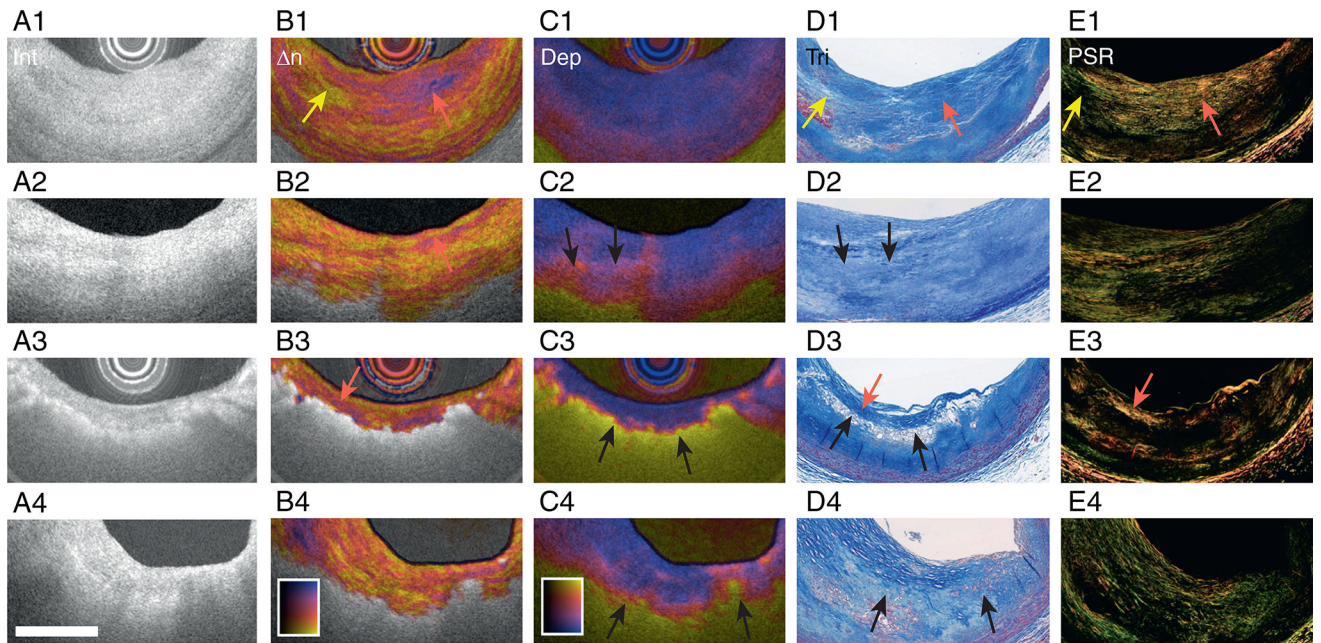
section, as indicated in the inset in **(A)** for the current example (see Figure 6 for tissue type legend). Scale bar in **(A)** measures 1 mm and applies to **(A to F)**. Scale bars in **(G to I)** measure 250 μm.

FIGURE 3. PS-OFDI of Lipid-Rich Plaque Regions

Plaque regions characterized by increased lipid content by histological examination correspond to areas of depolarization in polarization-sensitive optical frequency domain imaging (PS-OFDI). **(A)** Reflection intensity (Int), **(B)** birefringence (n), **(C)** depolarization (Dep), and **(D and E)** matching histological sections, stained with trichrome (Tri) and picrosirius red (PSR), respectively. The **first row** displays fibrotic tissue, where the birefringence corresponds closely to picrosirius red staining **(yellow and red arrows)**. The histological appearance of the early lesion in the **second row** suggests changes in the extracellular matrix organization and dispersed lipid, causing modest depolarization **(black arrows)**. The **third row** demonstrates the pronounced depolarization caused by an aggregation of foam cells in a more advanced lesion. The high birefringence in the fibrous cap matches picrosirius red staining **(red arrow)**. The **last row** shows depolarization caused by an advanced lesion with an extracellular lipid pool. Scale bar: 1 mm, applies to all panels.
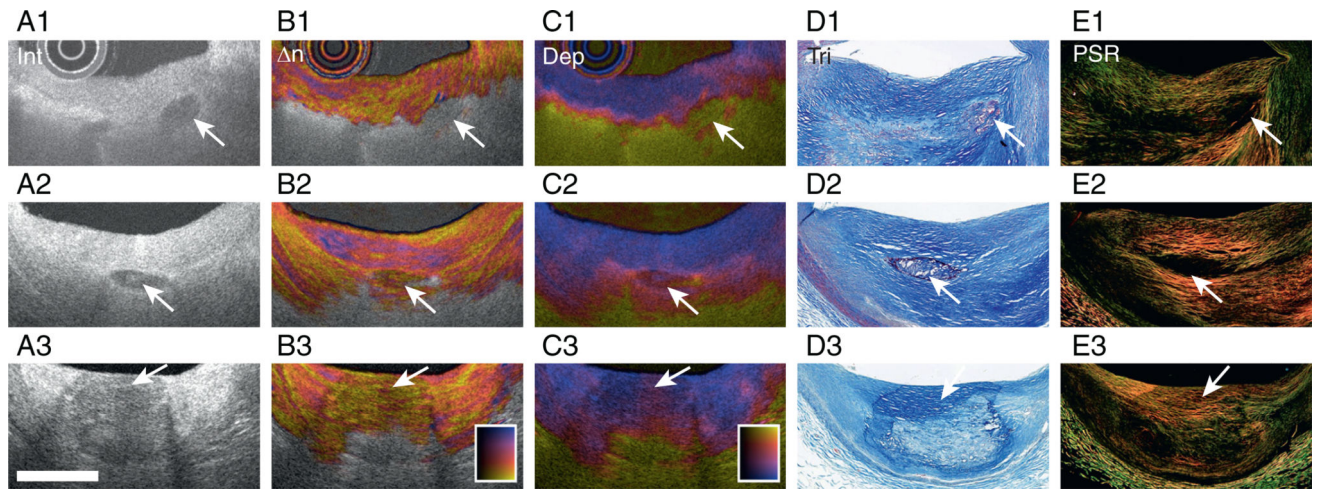
FIGURE 4. PS-OFDI of Calcifications

Calcifications **(white arrows)** may exhibit low birefringence close to the lumen, but they depolarize incident light, and that prevents evaluation of birefringence at greater depths. **(A)** Reflection intensity (Int), **(B)** birefringence (n), **(C)** depolarization (Dep), and **(D and E)** matching histological sections, stained with trichrome (Tri) and picrosirius red (PSR), respectively. In lipid-rich plaques **(first row)**, calcifications tend to depolarize more strongly than when surrounded by fibrous tissue **(second and third rows)**. Scale bar: 1 mm, applies to all panels.
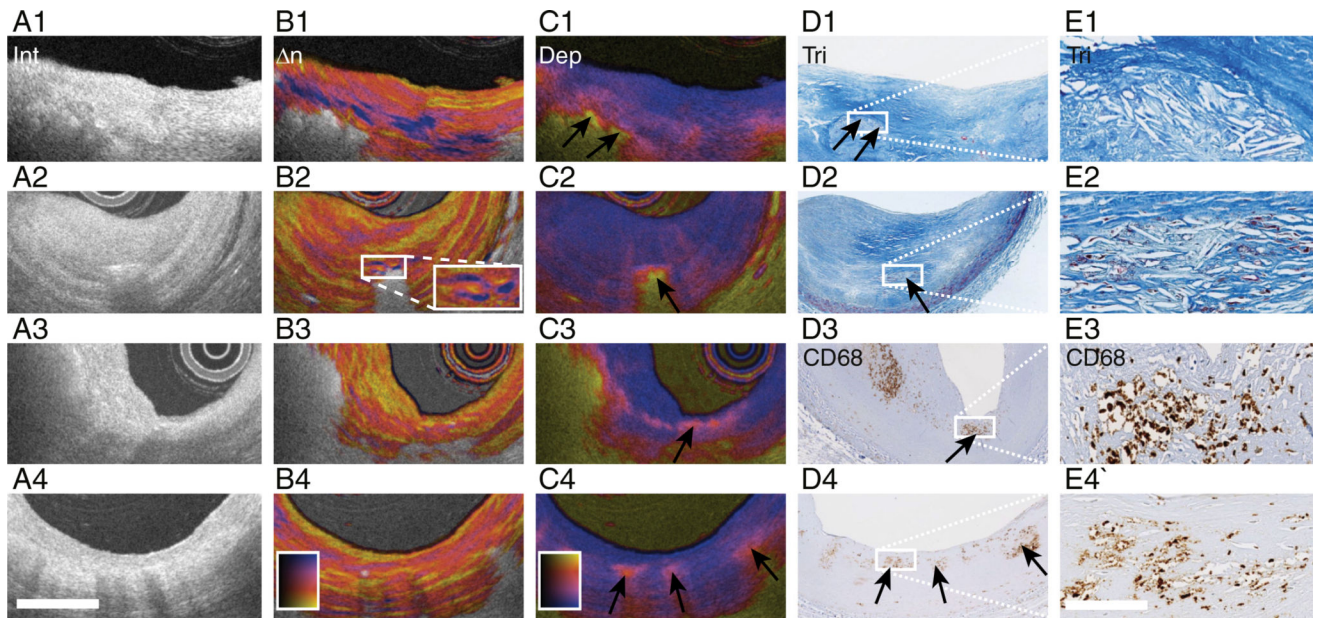
FIGURE 5. Polarization Signatures of Cholesterol Crystals and Macrophages
(A) Reflection intensity (Int), **(B)** birefringence (n), **(C)** depolarization (Dep), and **(D)** and **(E)** matching histological sections, stained with trichrome (Tri) and CD 68, respectively. **(E)** Magnified views of the regions of interest indicated in **D**. **(A1 to E1)** Irregularly oriented cholesterol crystals **(black arrows)** cause depolarization. **(A2 to E2)** Crystals oriented parallel to the lumen **(black arrow)** still depolarize, but they also create zones of high birefringence **(inset)**. **(A3 to E4)** Accumulations of macrophages **(black arrows)** cause depolarization, without entirely randomizing the detected polarization states. Scale bar: 1 mm for **(A to D);** 125 μm for **(E)**.
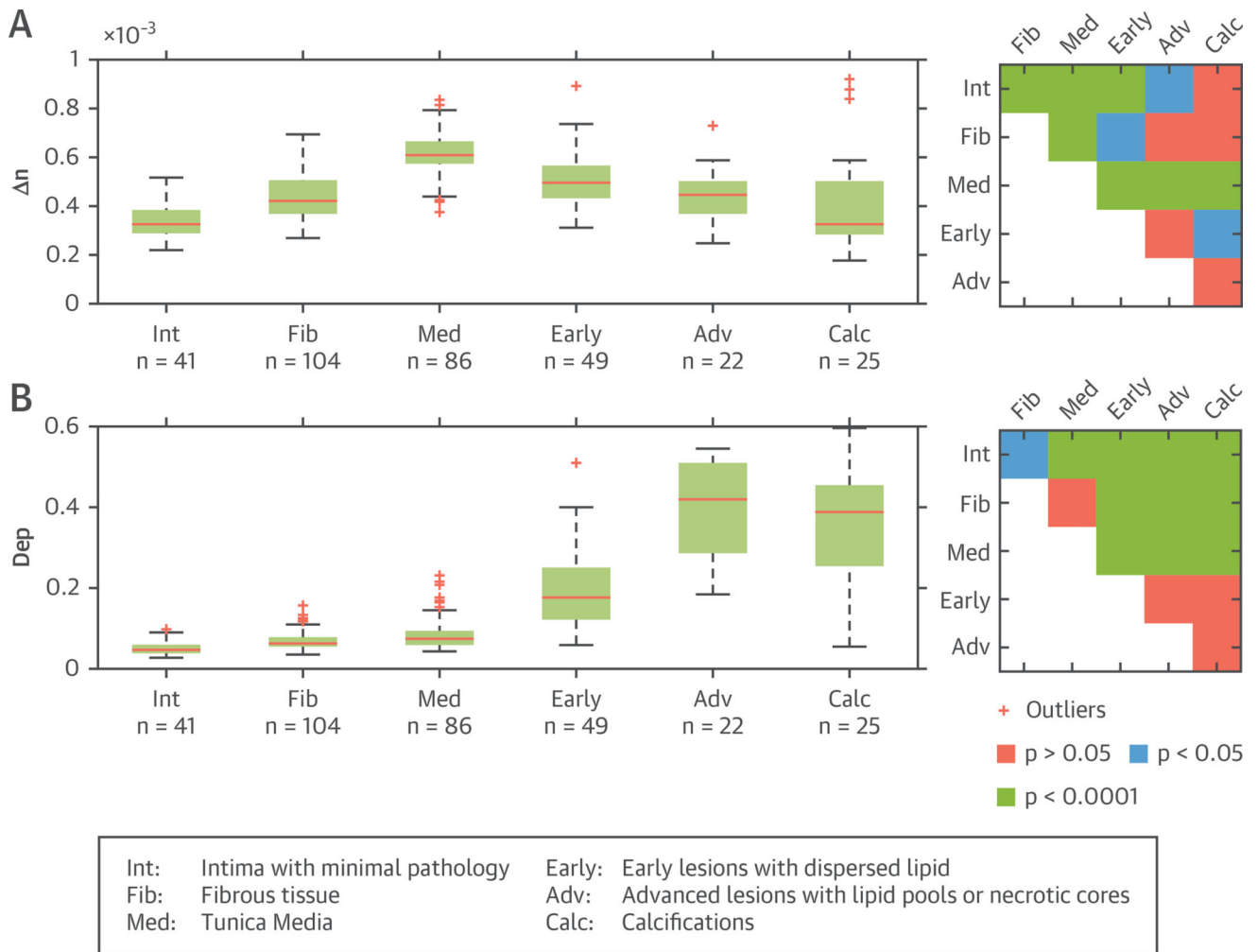
FIGURE 6. Quantitative Characterization of Tissue Polarization Properties
(A) Median and quartile birefringence (n) values in regions with depolarization 0.2 differed significantly across tissue types (p < 0.0001, 1-way analysis of variance). Intima with minimal abnormality had the lowest birefringence, and the tunica media had the highest. Less complicated lesions featured slightly higher birefringence than fibrous tissue (significant) and advanced lesions with defined lipid pools and necrotic cores (insignificant). **(B)** Median and quartile depolarization (Dep) values differed significantly from each other (p < 0.0001, Kruskal-Wallis). Lipid-rich tissues and calcifications showed significantly higher depolarization than did fibrous tissues or the layers of the normal vessel wall. Whisker lengths correspond to approximately 2.7 times the standard deviation, and data points are drawn as outliers if outside this range.